Journal of Alloys and Compounds 540 (2012) 121–126

Contents lists available at SciVerse ScienceDirect

Journal of Alloys and Compounds

journal homepage: www.elsevier.com/locate/jalcom

First-principles study on the electronic structure of a $LiFePO_4$ (010) surface adsorbed with carbon

Peixin Zhang [a,*], Dongyun Zhang [a,b,*], Lei Huang [a], Qun Wei [c], Muchong Lin [a], Xiangzhong Ren [a]

[a] College of Chemistry and Chemical Engineering, Shenzhen University, Shenzhen 518060, PR China
[b] School of Materials Science and Engineering, Harbin Institute of Technology Shenzhen Graduate School, Shenzhen 518055, PR China
[c] School of Science, Xidian University, Xi'an 710071, PR China

ARTICLE INFO

Article history:
Received 2 May 2012
Received in revised form 26 May 2012
Accepted 8 June 2012
Available online 23 June 2012

Keywords:
Lithium-ion battery
Lithium iron phosphate
First-principles method
Carbon

ABSTRACT

The electronic structures of a $LiFePO_4$ (010) surface adsorbed with C are studied by a first-principles method based on DFT. The results show that the system is more stable when the $LiFePO_4$ (010) surface is cut through Li atoms. PDOS analysis shows that the electronic structure of atoms in the sub-surface is similar to that of atoms in the bulk. The unpaired electrons in Fe-*d* orbital play a key role in the changes in the microelectronic structure; these changes lower the band gap and generate new bands that favor the transfer of electrons. Atom C reacts with Fe by chemisorptions when C is adsorbed on the outermost layer. Therefore, the materials may have better electrochemical properties by the improvement of diffusion of both electrons and Li ions when limiting the crystal growth with C coating.

1. Introduction

According to the working principles of the lithium battery, the battery's electrical conductivity strongly influences its electrochemical performance. An increase in the conductivity between the electrode's crystallites improves lithium diffusion and can improve the battery's high-rate performance. $LiFePO_4$ modified with a carbon (C) coating can enhance a battery's apparent conductivity and reduce the polarization [1–3]. This type of material can also provide electronic tunnels, balance the charge in the course of Li^+ intercalation, and thus improve the charge–discharge properties [4–8]. Huang et al. [9] have prepared carbon-coated $LiFePO_4$ materials with good rate capability and stability; they postulated that both particle-size minimization and intimate carbon contact were necessary to optimize the electrochemical performance. However, most of the research was only conducted by analysis of the battery performance; the mechanism of the carbon coating underlying the improved performance, particularly the relationship between the coating C layer and the interface of the $LiFePO_4$ material, has not been clearly determined. Therefore, it is important to perform studies on carbon-encapsulated $LiFePO_4$.

The geometric structure and electronic properties of the $LiFePO_4$ surface can be studied at the atomic scale through a first-principles calculation to allow enhanced understanding of the nature of the material's surface [10–13]. Ouyang et al. [14] have studied the stability and electronic structure of the $LiFePO_4$ (001), (010) and (100) surfaces; they concluded that the surface electronic structures of the (001) and (100) surfaces are metallic due to the contribution of surface P and Fe atoms. The (010) surface exhibits the most stable termination, which favors the lithium diffusion in the one-dimensional pathway. The electronic structure of the $LiFePO_4$ (010) surface is quite similar to that of the bulk. Wang et al. [15] have studied nine surfaces of $LiFePO_4$: (001), (010), (100), (011), (110), (101), (111), (201) and (301). Their results showed that the (010) and (201) surfaces exhibited the lowest energies. The experimental research of Chen [16] has shown that a crystal with the (010) surface was most easily produced.

In this paper, a computer calculation method of first-principles pseudo-potentials is used to explore the properties of C-coated $LiFePO_4$. The geometric structure and electronic characteristics of the $LiFePO_4$ (010) surface were the primary focus of the investigation. By comparing the calculation results of the band gap, conductive properties, and formation energy between the adsorption surface and the bulk material, we reveal the mechanism of carbon adsorption on the $LiFePO_4$ (010) surface, explain why the change in the microscopic structure can improve the electrochemical performance of $LiFePO_4$, and provide a theoretical foundation for large-scale production.

2. Research methods

Calculations were performed using the CASTEP program, [17] an *ab-initio* quantum program based on density functional theory (DFT). The cut-off energy of the plane wave was set at 500 eV in the reciprocal K-space. All calculations were per-

---

* Corresponding authors. Tel.: +86 755 26558134; fax: +86 755 26558134 (P. Zhang), tel.: +86 755 26538293; fax: +86 755 26536141 (D. Zhang).

E-mail addresses: pxzhang96@yahoo.com (P. Zhang), zdy_89@126.com (D. Zhang).

0925-8388/$ - see front matter © 2012 Elsevier B.V. All rights reserved.
http://dx.doi.org/10.1016/j.jallcom.2012.06.049

formed within the generalized gradient approximation (GGA) proposed by Perdew, Burke and Ernerhof (PBE) [18] for the exchange-correlation energy. A 2 × 5 × 1 k-point mesh was chosen to ensure the total ground-state energy converged using the Monkhorst–Pack method [19]. The SCF of every atom was set at 1.0×10^{-6} eV using the Pulay density mixing method in the SCF calculation. The Broyden–Fletcher–Goldfarb–Shanno (BFGS) algorithm [20] was applied to optimize the model.

The lattice parameters of the relaxed bulk $LiFePO_4$ structure are $a = 10.3185$ Å, $b = 6.0120$ Å, and $c = 4.7089$ Å, which agree well with experimentally determined values [21]. The initial unrelaxed (0 1 0) surface structures are carved out of the fully relaxed bulk crystal, as shown in Fig. 1(a). The thickness of the vacuum layer is 15 Å. According to the test results of the determination of energy vs. the height of surface layers [22], when the intercept depth is 12.024 Å with a total number of ions in cell of 56, the change of energy is small. Therefore, a slab of 12.024 Å with a relaxation layer of 3.9 Å is sufficient to achieve a converged surface energy considering the precision and efficiency of the computations. In our study, only atoms near the surface are allowed to relax until the forces are smaller than 0.03 eV/Å. The inner part of the slab is frozen at bulk positions to simulate the bulk of this material.

Three different models of C adsorbed on the $LiFePO_4$ (0 1 0) surface were considered. The original fractional coordinates are (0.5,0.5,0.5), (0,0.5,0.5), and (0.764,0.487,0.5). The fractional coordinates of C in Fig. 1(a) are (0.5,0.5,0.5).

Carbon-coated $LiFePO_4$ battery cathode material was prepared via the mechanical activation–high-temperature solid-phase method, and citric acid (A.R.) was used as the carbon source. A piece of lithium metal was used as the negative electrode of the battery. The capacity and cycle performance were tested via the constant-current charge–discharge method with a voltage that ranged from 2.6 to 4.2 V.

The XPS data were acquired using an ESCALAB 250 X-ray photoelectron energy disperse spectroscope (Thermo Fisher Scientific). This system uses monochromatized Al-Kα radiation (Mono AlKα) as the excitation source. The analysis room vacuum is approximately 2×10^{-9} mbar when the X-ray machine is operated. The entire spectrum scanning passes can be up to 150 eV and the narrow-spectrum scanning passes can be up to 20 eV, and the C1s of the surface contamination were used for the standard energy adjustment.

3. Results

3.1. Effect of cut position

$LiFePO_4$ crystallizes in space group *Pnma*; each unit cell contains four formula units. The positions of Fe2, Fe3 and Fe4 can be deduced from Fe1(x,y,z) by the symmetry operators ($-x + 1/2, -y, z - 1/2$), ($-x, y + 1/2, -z$), and ($x + 1/2, -y + 1/2, -z + 1/2$) according to an analysis of the Wyckoff positions.

Different cases of exposed atoms can be obtained when surface (0 1 0) is cut from bulk $LiFePO_4$. For example, when the (0 1 0) surface is cut through (0,0,0) and (0,1/2,0), Li and O atoms will be exposed at the surface. When the (0 1 0) surface is cut through (0,1/4,0) and (0,3/4,0), Fe, P and O atoms will be exposed at the surface. The stability of the system varies depending on the exposed atoms, and adsorption occurs only at the most stable cleaving surface. Therefore, relaxation of all these possible cut surfaces is necessary to determine the surface with the lowest surface energy for further adsorption calculations. Based on the symmetrical structure of the $LiFePO_4$ space group, the cleave surfaces that are cut through (0,0,0) and (0,1/2,0) are similar to cuts (0,1/4,0) and (0,3/4,0). Therefore, the two possibilities of termination cleaving—at (0,0,0) and (0,1/4,0)—are calculated where possible. The results show that the energy of the optimized structure is $E_{(0,0,0)} = -2.1053 \times 10^4$ eV and $E_{(0,1/4,0)} = -2.1045 \times 10^4$ eV.

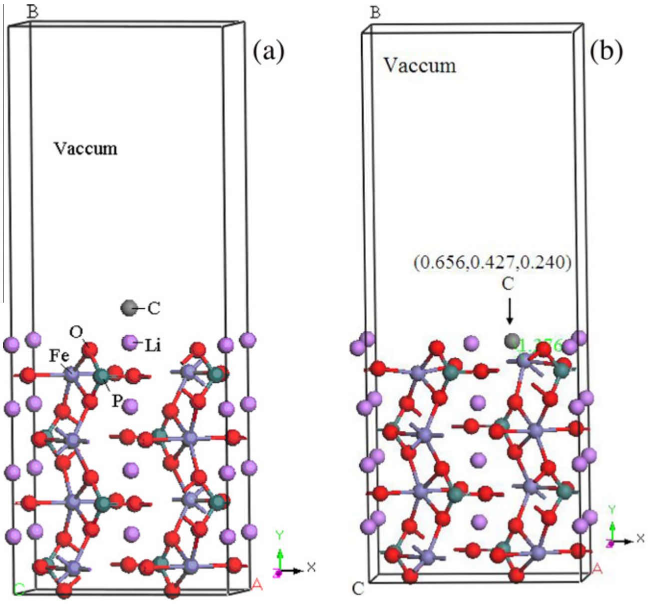

Fig. 1. Slab model of the $LiFePO_4$ (0 1 0) surface with C adsorption (a) initial and (b) relaxed structure.

3.2. Surface relaxation of $LiFePO_4$ (0 1 0)

The band structure of $LiFePO_4$ at the Fermi level is shown in Fig. 2(a). The band gap is 1.23 eV, which is smaller than the calculated one of the bulk (2.38 eV). Three new bonds formed (No. 160–162) at the Fermi level. Generally, there's always an underestimate for the band gap calculated by the first principles. Usually we do not care about absolute value. Instead, we care about the differences. So it is not that important if two methods show different absolute band gap.

The DOS of $LiFePO_4$ surface (0 1 0) is shown in Fig. 3. A large difference is observed between the bulk and the surface, but little difference is observed between the bulk and the sub-surface. Analysis of the atomic PDOS on the surface region and the bulk material reveals only small changes for the Li and P atoms. The PDOS of Fe at different positions varies substantially, as shown in Fig. 4(a). Fe4,

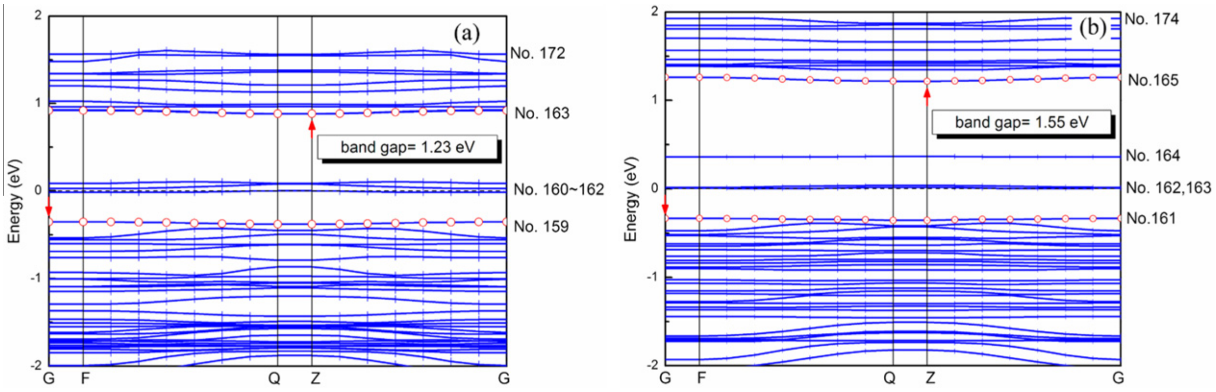

Fig. 2. Band structure at the Fermi level for (a) $LiFePO_4$ (0 1 0) and (b) C–$LiFePO_4$ (0 1 0).

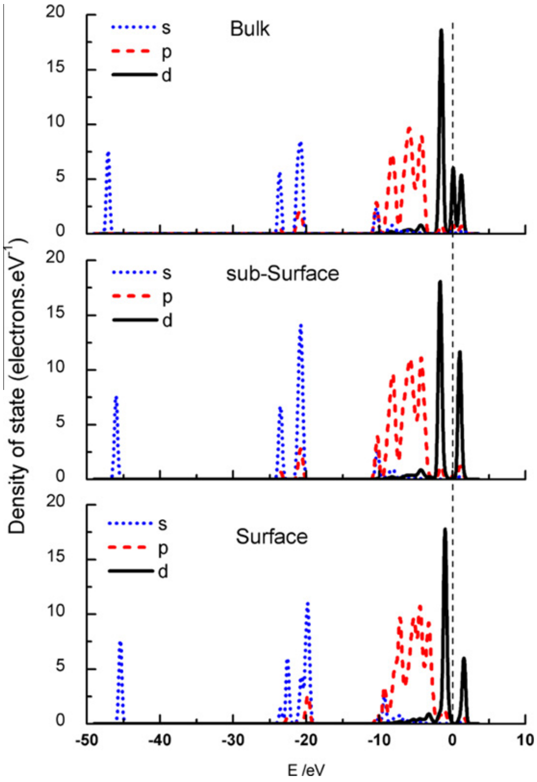

Fig. 3. Density of states of $LiFePO_4$ surface (0 1 0).

Fe2, Fe3 and Fe1 represent iron atoms located at the surface, the sub-surface, and the bulk. Only the PDOS of Fe4 differs greatly.

The calculated population results of $LiFePO_4$ are listed in Table 1. Fe3 atoms bond with six O atoms to form $[FeO_6]$ octahedra in the bulk. However, atom Fe4, which is terminated at the surface, only bonds with five O atoms to form $[FeO_5]$ octahedra because of the broken Fe–O3 bond.

3.3. $LiFePO_4$ surface (0 1 0) adsorbed with C

Surface (0 1 0) modeled with C after relaxation is shown in Fig. 1(b). The fractional coordinates of C changed from (0.5, 0.5, 0.5) to (0.656, 0.427, 0.240), which is very close to the position of Fe6 (0.705, 0.388, 0.077) in surface-terminated sites. Other calculated results, including the population analysis, are shown in Table 2, column C1.

Surface adsorption energy (ΔE_a) is defined as follows:

$$\Delta E_a = E(\text{surface after adsorption}) - E(\text{surface without adsorption}) - E(\text{adsorbate})$$

Therefore, the surface adsorption energy for the system depicted in Fig. 1(b) is $\Delta E_a = E_{\text{C-on-(010)}} - E_{(010)} - E_{\text{C}} = (-2.121 \times 10^4) - (-2.105 \times 10^4) - (-1.466 \times 10^2) = -7.082$ eV.

The shortest bond in Fig. 1(b) is C–Fe6 according to the population analysis: bond length = 1.376 Å, population = 1.21. The bond lengths of C–Li and C–O are 2.226 Å and 2.678(∼2.989) Å respectively, and the populations of these two bonds are 0.

If the original fractional coordinates of C are set at (0, 0.5, 0.5) and (0.764, 0.487, 0.5) (just above Fe6), the fractional coordinates of relaxed C are (0.156, 0.427, 0.261) and (0.655, 0.427, 0.240), which are close to the coordinates of Fe4 (0.204, 0.388, 0.423) and Fe6 (0.704, 0.388, 0.077) in the surface-terminated sites (shown in Table 2, columns C2 and C3). The shortest bond for C adsorbed at C2 and C3 are C–Fe4 and C–Fe6 respectively: bond length = 1.376 Å, population = 1.21.

The microstructure varies little with the position of C. The band structure at the Fermi level of $LiFePO_4$ surface (0 1 0) adsorbed with C, i.e., the relaxed structure shown in Fig. 1(b), is shown in Fig. 2(b). A comparison of the band structures indicates that the number of conduction bands (No. 165–174) remains unchanged and that the band gap (1.55 eV) is larger than that of $LiFePO_4$ surface (0 1 0) (1.23 eV) but still less than that of $LiFePO_4$ bulk (2.38 eV). Three new bands (No. 162–164) appear at the Fermi level.

Table 1
Calculated population results of $LiFePO_4$ (0 1 0).

Fe–O	Type of O	Population	Bond length (Å)
Surface (0 1 0) [FeO_5]			
O 022–Fe 004	O1	0.22	2.1503
O 024–Fe 004	O2	0.24	2.1404
O 004–Fe 004	O3	0.20	2.1267
O 016–Fe 004	O3	0.14	2.1363
O 014–Fe 004	O3	0.25	2.0461
Bulk [FeO_6]			
O 021–Fe 003	O1	0.23	2.2006
O 023–Fe 003	O2	0.24	2.1279
O 002–Fe 003	O3	0.20	2.1530
O 013–Fe 003	O3	0.27	2.1530
O 003–Fe 003	O3	0.16	2.1834
O 015–Fe 003	O3	0.18	2.1834

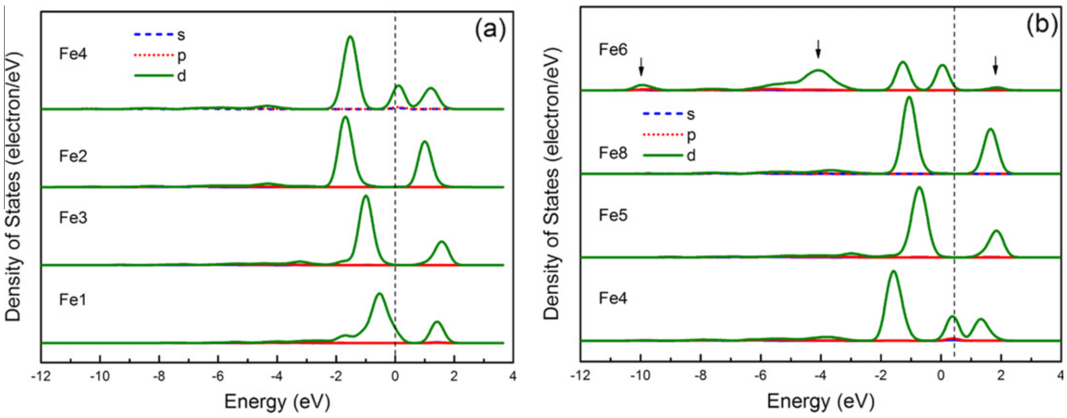

Fig. 4. PDOS of Fe at different positions in (a) $LiFePO_4$ (0 1 0) and (b) C–$LiFePO_4$ (0 1 0).

Table 2
Calculated results of $LiFePO_4$ (0 1 0)/C.

	C1	C2	C3
Fractional coordinates of C			
Original	(0.5, 0.5, 0.5)	(0, 0.5, 0.5)	(0.764, 0.487, 0.5)
Relaxed	(0.656, 0.427, 0.240)	(0.156, 0.427, 0.261)	(0.655, 0.427, 0.240)
Fractional coordinates of Fe bonded with C	Fe6 (0.705, 0.388, 0.077)	Fe4 (0.204, 0.388, 0.423)	Fe6 (0.704, 0.388, 0.077)
C–Fe :			
Bond length (Å)	1.3758	1.3756	1.3759
Population	1.21	1.21	1.21
ΔE_a (eV)	−7.082	−7.081	−7.082
Band gap (eV)	1.548	1.548	1.546

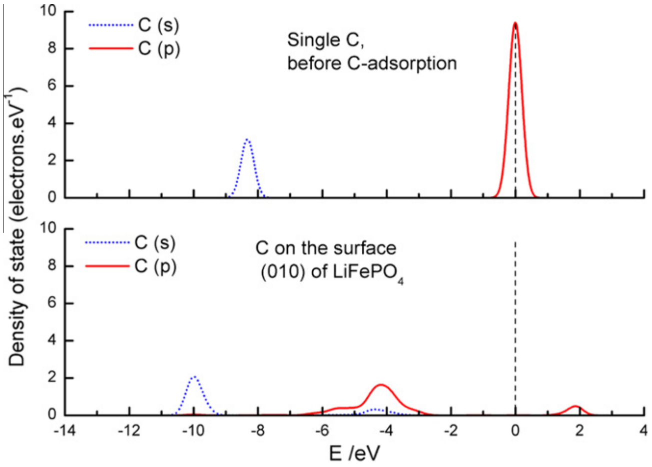

Fig. 5. PDOS of C before and after adsorption.

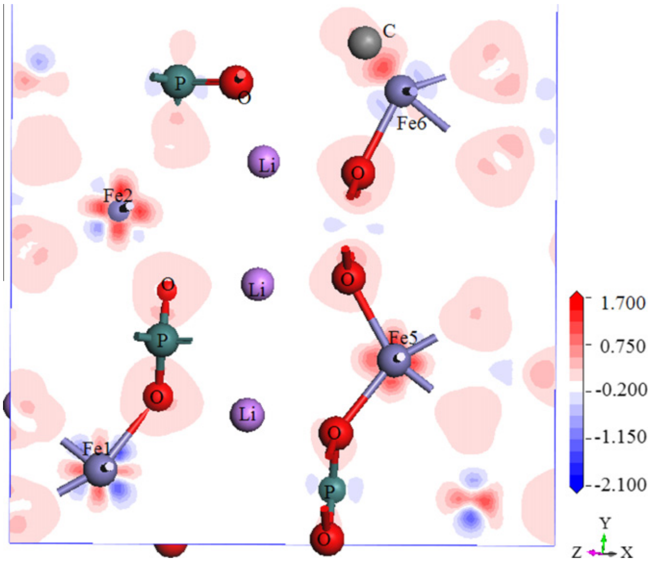

Fig. 6. Electron-density difference of surface (0 1 0) adsorbed with C (Fe6 locates at the surface and bonds with C, Fe2 is in the sub-surface, and Fe5 and Fe1 are in the bulk).

The DOS analysis of this system shows that it is very similar with the DOS analysis of $LiFePO_4$ surface (0 1 0) shown in Fig. 3, and only orbital d near the Fermi level appears differently. Thus further analyses concerning C and Fe in different situations are discussed in the following.

Fig. 4(b) compares the PDOS of Fe located at different sites, where Fe4, Fe5, Fe6 and Fe8 represent Fe located at the surface without adsorption, the bulk, the surface with adsorption, and the sub-surface, respectively.

The PDOS of C before and after adsorption is shown in Fig. 5. The s and p orbitals of the single C are located at −8 and 0 eV. The energy of the adsorbed C is lowered, and the p orbital is dispersed at −4 and 2 eV.

The electron-density difference map of $LiFePO_4$ surface (0 1 0) adsorbed with C, cut though C–Fe6, is shown in Fig. 6. In the figure, blue represents a lack of electrons, and red represents a gathering of electrons.

4. Discussion

4.1. Effect of cut position

The lower the energy, the more stable the system. According to our calculations, $E_{(0,0,0)} < E_{(0,1/4,0)}$, surface (0 1 0) cleaved at (0, 0, 0) is more stable than the surface cleaved at (0, 1/4, 0) because both surfaces have a same surface area. On the other hand, the energy should be very high if the surface is cleaved through the highly covalent P–O in PO_4 tetrahedron. The PO_4 tetrahedron is preserved when the surface is cut through (0, 0, 0). All subsequent simulations will therefore be based on this surface.

Experimentally, the electrochemical properties of $LiFePO_4$ are improved when small particles are used, due to shorter diffusion distance of Li ions in the particles. In general, only the direction of growth can be determined by the experimental method. It is not easy to determine the exposed atoms by the experimental method. The results of this study show that the top of the terminal surface favors exposed Li. This means that the smaller the particles, more Li are exposed on the terminal surface and the transfer of Li between particles is favorable too. These results help explain the improvement in the properties of $LiFePO_4$ when small particles are used.

4.2. Electronic structure of $LiFePO_4$ (0 1 0) surface

From Figs. 3 and 4(a), the new bands at the Fermi level in Fig. 2(a) are created because of the effects on the d orbitals which exist only in the Fe atoms. Surface (0 1 0) forms only 5 Fe–O bonds, whereas the Fe in the bulk forms 6 Fe–O bonds. The breakage of Fe–O bonds at the surface increases the activity of Fe and leads to a dramatic increase in the number of electrons in the Fe-d orbital and to new bonds at the Fermi level.

The results of Rousse [23] have indicated that Fe atoms in $LiFePO_4$ are high-spin (weak field). According to crystal-field theory, the five d orbitals form different degenerate orbitals in the non-spherically symmetrical ligand field. The spin configuration of Fe-

$3d^6$ is $4t_{2g}2e_g$. Orbital t_{2g} contains three spin-up electrons and one spin-down electron; these electrons bonds with electrons in the *p* orbitals of four O3 atoms. The two spin-up electrons in orbital e_g bond with electrons in the *p* orbitals of O1 and O2.

The lowered band gap and the new formed bonds both favor the transfer of electrons from the valence band through the forbidden band to the conduction band. So if small particles are used, the electrochemical properties of $LiFePO_4$ can be improved due to the better transfer of the electrons too.

4.3. Electronic structure of $LiFePO_4$ (010) surface adsorbed with C

The surface adsorption energy (refer to Table 2) decreased, which means the system is more thermodynamically stable after C adsorption. The relaxed system energies are almost equal, irrespective of the original fractional coordinates of C. The same is true for the surface adsorption energy, which means the systems are all stable.

The new bands (No. 162–164 in Fig. 2(b)) at the Fermi level are important for the improvement in the ability of electrons to jump from the upper valence band to the conduction band.

The PDOS of atom Fe (shown in Fig. 4(b)) differs significantly between the sites. For example, the electrons in orbital Fe5-*d* in the bulk material separate, which leads to a large band gap and poor conductivity. The electron energy of orbital Fe4-*d*, which lies in $LiFePO_4$ surface (010) and does not bond with C, is relatively high, and the electrons in the conduction band apparently separate from each other near the Fermi level. The electrons in orbital Fe6-*d*, which lies in $LiFePO_4$ surface (010) and bonds with C, exhibit a low energy, and both electrons separate. The energy positions at −10, −4 and 2 eV of Fe6 match those of C (Fig. 5). The major contribution arises from orbitals C-*p* and Fe-*d*. Thus, band No. 164 in Fig. 2(b) is formed by orbital C-*p*.

According to the atomic population values, Fe6 (7.50) > Fe4 (7.10) > (Fe2, Fe3, Fe5, Fe8) (7.09) > (Fe1, Fe7) (6.94). The atom with the largest charge is Fe6, which bonds with C. At the same time the bond population (Table 2) analyze also show the covalent interactions of Fe–C are stronger than those of Fe–O because the electronic structure is different between C and O. As discussed previously in relaxed surface (010), these bond lengths are attributable the broken Fe–O bonds. The covalent interactions of C–Li and C–O are weaker due to the relatively longer bond length. As evident in Fig. 6, strong covalent interactions exist between Fe6 and C, which may leads to a more stable structure. These interactions differ from those of Fe–O in the bulk, where the Fe–O interactions show good symmetry because Fe5 and Fe1 bond with O atoms to form $[FeO_6]$ octahedra. All the evident show that chemisorptions occur and lead to easier adsorption of C.

The binding energies of Li, Fe, P and O in experimental synthesized $LiFePO_4$/C, as determined using X-ray photoelectron spectroscopy (XPS), are shown in Table 3. Only the spectrum of Fe-2*p* consists of two different-strength peaks. The spectrum shows that the binding energy increases, except for that of P-2*p* and O-1*s*. The binding energy of Fe increases due to the large electronegativity of P and O. Similarly, the binding energy of C increases because the electronegativity of C is between that of P and O and because the content of O is greater than that of P. The XPS results for Fe differ from the theoretical value because of the low electronegativity of Fe. The increase in the binding energy of the whole system means that the coated carbon atoms bond with $LiFePO_4$ through chemisorptions, which agrees with the simulation results.

Table 3
Binding energy of each element in $LiFePO_4$/C.

	Fe-2*p*		O-1*s*	C-1*s*	P-2*p*	Li-1*s*
	2*p*1	2*p*3				
Binding energy (eV)	723.9	711.5	531.55	284.8	133.5	55.4
Theoretical value (eV)	719.9	706.7	531.8	285.0	130.6	54.9
Δ (eV)	4.0	4.8	−0.25	0.8	−0.1	0.5

According to crystal chemistry theory, the smaller the particle size, the larger the specific surface area, which may cause a high surface energy and a thermodynamically unsteady state, and the easier it is to gather to form dough. So citric acid is added during the real synthesis process. It is believed that citric acid pyrolyzes to form a carbon-coating space barrier and inhibits the growth of secondary crystalline particles to some extent. From our calculation, the transfer of electrons is improved for the decrease in the band gap and the generation of new bands relative to the bulk. Therefore, the electrochemical properties of $LiFePO_4$/C were improved because the amounts of surface ingredients increased as the particle size was reduced and the particles were coated with C. The theoretical result was consistent with the experimental data.

Experimentally, two main factors account for the improved electrochemical performance of carbon-coated $LiFePO_4$. First, the carbon can form a carbon network structure with good electrical conductivity on the surface of $LiFePO_4$. This network structure not only strengthens the inter-particle contacts but also improves the conductivity between particles. These stronger contacts provide a better electronic transmission channel, reduce the polarization, reduce capacity fading and improve the reversibility of the charge–discharge processes [9,24]. Second, the carbon membrane layer helps restrain the growth of crystal grains, thereby decreasing crystal size and increasing the specific surface area [25,26], which shortens the path of the embedded Li^+ and improves the Li^+ diffusion coefficient. Furthermore, the contact area of the electrolyte increases with an increase in the specific surface area, as does the Li^+ diffusion area between the phases. Recently, $LiFePO_4$ coated with SiO_2 [27] has been studied, and it shows good electrochemical properties the same as carbon coated $LiFePO_4$.

In this work, only one C adsorbed on the (010) surface of $LiFePO_4$ was studied. There are still a lot of work to do in the future, including C adsorbed on other surfaces and the adsorbed amount.

5. Conclusions

The electronic structures of $LiFePO_4$ adsorbed with C are studied by first-principles method based on DFT. The results are as follows:

(1) The more stable surface is $LiFePO_4$ (010) with Li exposed, which benefits the phase transfer and enhances the diffusion of Li^+.
(2) The PDOS analysis shows the electronic structures of atoms in the sub-surface are similar to the structures of atoms in the bulk. Only the positions of atoms at the surface change significantly. The unpaired electrons in Fe-*d* orbital play a key role in the changes in the microelectronic structure, which lowers the band gap and generates new bands to favor the transfer of electrons. Therefore, the electrochemical properties can be improved by limiting the growth of the crystallites.
(3) The simulation results show that C reacts with Fe by chemisorptions when C is adsorbed on the outermost layer, which leads to easy adsorption.

Acknowledgments

This work was supported by the National Natural Science Foundation of China (Nos. 50874074, 51110105014, and

50474092), the Natural Science Foundation of Guangdong Province, China (No. 8151806001000028), Shenzhen Government's Plan of Science and Technology (Nos. ZYC200903250150A and 200505), Open Research Fund of Shenzhen Key Laboratory of Functional Polymer (FP20110004). This work was supported by Shanghai Supercomputer Center of China. Software CASTEP was supported by Hunan University.

References

[1] M. Yang, Q. Gao, J. Alloys Compd. 509 (2011) 3690–3698.
[2] R. Dominko, M. Gaberscek, J. Drofenik, M. Bele, S. Pejovnik, J. Jamnik, J. Power Sources 119–121 (2003) 770–773.
[3] R. Dominko, M. Bele, J.M. Goupil, M. Gaberscek, D. Hanzel, I. Arcon, J. Jamnik, Chem. Mater. 19 (2007) 2960–2969.
[4] H. Gabrisch, J.D. Wilcox, M.M. Doeff, Electrochem. Solid-State Lett. 9 (2006) A360–363.
[5] X. Zhi, G. Liang, L. Wang, X. Ou, L. Gao, X. Jie, J. Alloys Compd. 503 (2010) 370–374.
[6] M. Gaberscek, M. Küzma, J. Jamnik, Phys. Chem. Chem. Phys. 9 (2007) 1815–1820.
[7] K. Kim, Y.H. Cho, D. Kam, H.S. Kim, J.W. Lee, J. Alloys Compd. 504 (2010) 166–170.
[8] J.K. Kim, J.W. Choi, G. Cheruvally, J.U. Kim, J.H. Ahn, G.B. Cho, K.W. Kim, H.J. Ahn, Mater. Lett. 61 (2007) 3822–3825.
[9] H. Huang, S.C. Yin, L.F. Nazar, Electrochem. Solid-State Lett. 4 (2001) A170–A172.
[10] G. Ceder, Y.M. Chiang, D.R. Sadoway, M.K. Aydinol, Y.I. Jang, B. Huang, Nature 392 (1998) 694–696.
[11] S.Q. Shi, C.Y. Ouyang, Z.H. Xiong, L.J. Liu, Z.X. Wang, H. Li, D.S. Wang, L.Q. Chen, X.J. Hunag, Phys. Rev. B: Condens. Matter 71 (2005) 144404–144409.
[12] F. Zhou, M. Cococcioni, C.A. Marianetti, D. Morgan, G. Ceder, Phys. Rev. B: Condens. Matter 70 (2004) 235121.
[13] F. Zhou, K. Kang, T. Maxisch, G. Ceder, D. Morgan, Solid State Commun. 132 (2004) 181–186.
[14] X. Ouyang, M. Lei, S.q. Shi, C. Luo, D. Liu, D. Jiang, Z. Ye, M. Lei, J. Alloys Compd. 476 (2009) 462–465.
[15] L. Wang, F. Zhou, Y.S. Meng, G. Ceder, Phys. Rev. B: Condens. Matter 76 (2007) 165435.
[16] G. Chen, T. Richardson, ECS Meeting Abstracts 702 (2007) 642.
[17] M.D. Segall, P.J.D. Lindan, M.J. Probert, C.J. Pickard, P.J. Hasnip, S.J. Clark, M.C. Payne, J. Phys.: Condens. Matter 14 (2002) 2717–2744.
[18] J.P. Perdew, K. Burke, M. Ernzerhof, Phys. Rev. Lett. 77 (1996) 3865–3868.
[19] H.J. Monkhorst, J.D. Pack, Phys. Rev. B: Condens. Matter 13 (1976) 5188.
[20] T.H. Fischer, J. Almlof, J. Phys. Chem. 96 (1992) 9768–9774.
[21] O.V. Yakubovich, M.A. Simonov, N.V. Belov, Dokl. Akad. Nauk SSSR 235 (1977) 93–95.
[22] J.L. Nie, H.Y. Xiao, F. Gao, X.T. Zu, J. Alloys Compd. 476 (2009) 675–682.
[23] G. Rousse, J. Rodriguez-Carvajal, S. Patoux, C. Masquelier, Chem. Mater. 15 (2003) 4082–4090.
[24] F. Brochu, A. Guerfi, J. Trottier, M. Kopeć, A. Mauger, H. Groult, C.M. Julien, K. Zaghib, J. Power Sources 214 (2012) 1–6.
[25] K. Yang, Z. Deng, J. Suo, J. Power Sources 201 (2012) 274–279.
[26] F. Pan, W.-l. Wang, H. Li, X. Xin, Q. Chang, W. Yan, D. Chen, Electrochim. Acta 56 (2011) 6940–6944.
[27] Y.-D. Li, S.-X. Zhao, C.-W. Nan, B.-H. Li, J. Alloys Compd. 509 (2011) 957–960.